Supporting Information (SI)

Mesoporous Titania Embedded PAN Composite Nanofibrous Membrane for Particulate Matter Filtration

P. Reena[a], N. Gobi [b], P. Chitralekha[c], D. Thenmuhil[a*], V. Kamaraj[a]

[1]Department of Ceramic Technology, Anna University, Chennai, 600 025, Tamilnadu, India.
[2]Department of Textile Technology, Anna University, Chennai, 600 025, Tamilnadu, India.
[3]Department of Bio-Technology, IIT Madras, Chennai – 600 025
*Corresponding Authors E-mail address: **muhil.ceramics@gmail.com**

Experiment

Materials

Polyacrylonitrile (PAN) (MW 150,000 g/mol) $(C_3H_3N)_n$, N, N-Dimethylformamide (DMF), Titanium isopropoxide (TIIP), cetyltrimethylammoniumbromide (CTAB) were purchased from Sigma Alrich. Dimethylformamide (DMF) was purchased from Merck India Pvt. Ltd.

Preparation and characterization of Mesoporous Titania

Hydrolysis and condensation of TTIP precursor was carried out in ethanol-water medium. Diluted nitric acid was added slowly to this to initiate the process along with the addition of pore directing agent CTAB keeping the molar ratio as 0.5 with respect to TTIP. This mixture was subjected to agitation overnight to achieve complete hydrolysis and condensation of alkoxide precursor. The resulted mixture was centrifuged and washed thoroughly with ethanol and finally with hexane to remove the excess precursors. In order to ascertain the suitable calcination temperature, thermo-gravimetric analysis (TGA) was carried out using thermal analyzer NETZSCH STA 449 F3 Jupiter from ambient temperature to 900 ºC at a heating rate of 10 °C/min.

The resulted white power was dried over night at 60 ºC and subjected to calcination at 500 ºC to achieve the formation of crystalline phases and removal of organic surfactant. The obtained mesoporous titania phases were confirmation using X-Ray diffractometer Rich Seifert-3000 (Germany) equipped with Copper anode target (Cu Kα radiation of wavelength, λ=1.54 Å). Further, the surface area and pore distribution were also measured using Micromeritics ASAP 2010 volumetric adsorption analyzer. Before the adsorption of N_2 gas, both the mesoporous titania sol and calcinated samples were subjected to complete dryness at 110 °C under vacuum in the degas port. BET isotherm was adopted to calculate the surface areas. Finally, the morphology of the prepared MT was analyzed using FEI Quanta FEG 200 – High resolution Scanning Electron Microscope in low vacuum mode equipped with Energy dispersive X-ray Spectrometry (EDX) microscope using 20 to 30 kV. HRTEM images were captured using a TECNAI G2 S-Twin transmission electron microscope with an acceleration voltage of 150 kV.

Principle of Construction of Membrane and characterization

The non-woven fabric with different areal density was used as supporting material to enhance the stability of the nanofibrous web of electrospun MT doped PAN solution. The pore size of the as prepared web was analyzed using Porous Material Inc. NY-14850, USA Hg porosimetry. The diameter and morphology of electrospun nanofibres were characterized by scanning electron microscope (HITACHI S-3400 SEM). The FTIR and Raman spectrum were also recorded for the resulted nanofibrous using Perkin Elmer 6X FT-IR Spectrometer, (Waltham, Massachusetts, USA) and HORIBA LABRAM HR800 UV (633 nm He-Ne laser source) instruments respectively. The air permeability of the prepared nanofibrous composites membranes were tested as per ASTMD737-04.

Principle of Construction of Membrane

The Principle of construction of membrane and its characterization are given the supporting information. The schematic representation of electro-spun is shown in Fig. S1a

and formation of multilayer polymeric nano composite membrane is also illustrated in Fig. S1b.

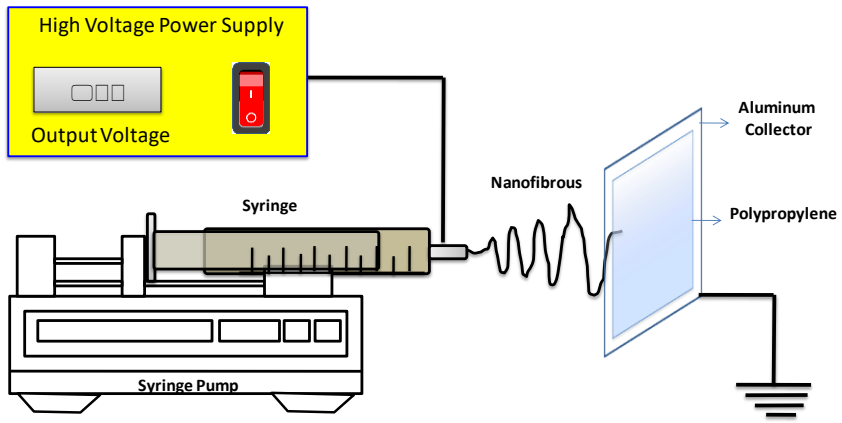

Fig. S1a Pictorial representation of the experimental setup for the preparation of nanofibrous PAN/MT

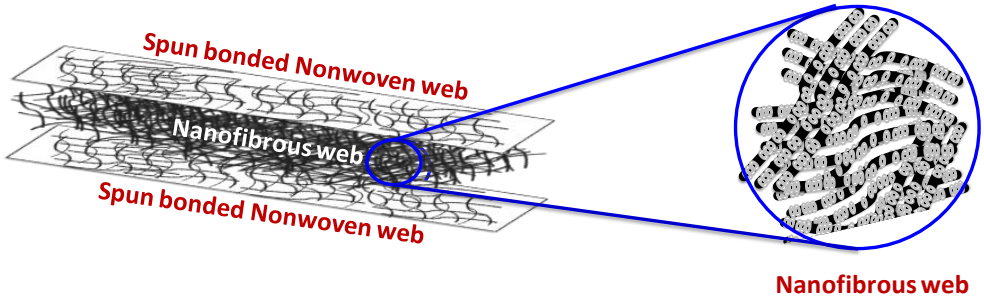

Fig. S1b Schematic representation of multilayer polymeric nanocomposite membrane

Filtration Analysis

NaCl aerosol particles were used to evaluate the filtration performance of the developed MT/PAN membranes. Fig. S1c illustrates the experimental setup for aerosol filtration efficiency tester**.** Initially, the clean air required for the experiments was obtained from compressor coupled with a pre-filter. Precision Air regulator was adopted to adjust the air flow and it was first split into two ways. The first one led to the aerosol generator and the second one to aerosol or dilution chamber. The aerosol neutralizer was not used in the

process to identify the effect of surface charge of MT nanoparticles with respect to the attraction of Na^+ and Cl^- charged aerosol. The prepared samples were held in 8 mm diameter filter holder. The process of measuring filtration efficiency was then carried out by maintaining uniform face velocity of 5 cm/s and difference in pressure was measured using a differential pressure gauge. Laser particle counter (Lasair III, Particle Measuring System) was used to measure the aerosol concentration at upstream and downstream from which the Aerosol Filtration Efficiency (AFE) was calculated using

$$\textbf{\% of AFE} = [(A-B)/A] \times 100$$

where 'A' is the number of aerosol concentration in upstream and 'B' is the number of aerosol concentration in downstream.

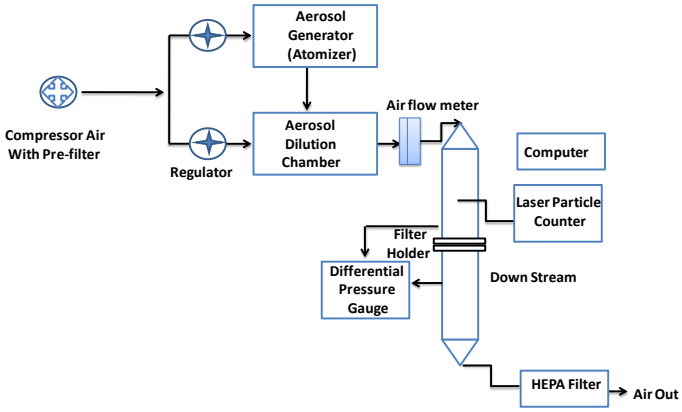

Fig. S1c Experimental setup for aerosol filtration efficiency tester.

Statistical Analysis

Regression Analysis

Here, a multiple polynomial regression equation (Equation 1) was used to derive the regression co-efficient to analyze the relationship between filtration efficiency with the three independent variables. The formed equations are presented in Table S1.

$$Y = b_0 + \sum_{i=1}^{3} b_i x_i + \sum_{\substack{i=1 \\ i<j}}^{3} b_{ij} x_i^2 + \sum_{i=1}^{3} b_{ij} x_i x_i \text{ ----------(1)}$$

where, b_0, b_i, b_{ij} are the Coefficients of regression equation, i and j are the integers and Y is the response to the independent variable.

Composite Desirability Analysis

Composite desirability has been evaluated based on which the optimum level of parameters. The desirability function analysis was carried out using Minitab 14 software.

Table S1 Regression equation for process variables

S.No	Property	Regression equation	R^2	F-Value
1.	Aerosol Filtration Efficiency	$Y= 174.45 - 10.285X_1 + 12.7X_2 - 0.061X_3 - 0.21\ X_1\ X_2 - 0.009X_2X_3 - 0.005X_2X_3 + 0.281X_1^2 - 1.325X_2^2 + 0.002312X_3^2$	0.09545	11.65
2.	Pore diameter	$Y = 1.032 - 0.06380X_1 - 0.0876X_2 - 0.0007X_3 - 0.00437X_1X_2 - 0.000105\ X_1X_3 - 0.00049X_2X_3 + 0.0030X_1^2 - 0.006X_2^2 - 0.000006X_3^2$	0.979	25.87
3	Air Permeability	$Y = 31.71 - 2.02X_1 - 91.955X_2 + 0.302X_3 - 0.066X_1X_2 - 0.0007\ X_1X_3 - 0.0545X_2X_3 + 0.0997X_1^2 - 0.8925X_2^2 - 0.0041X_3^2$	0.9909	60.77

Results and Discussion

Thermogravimetric Analysis

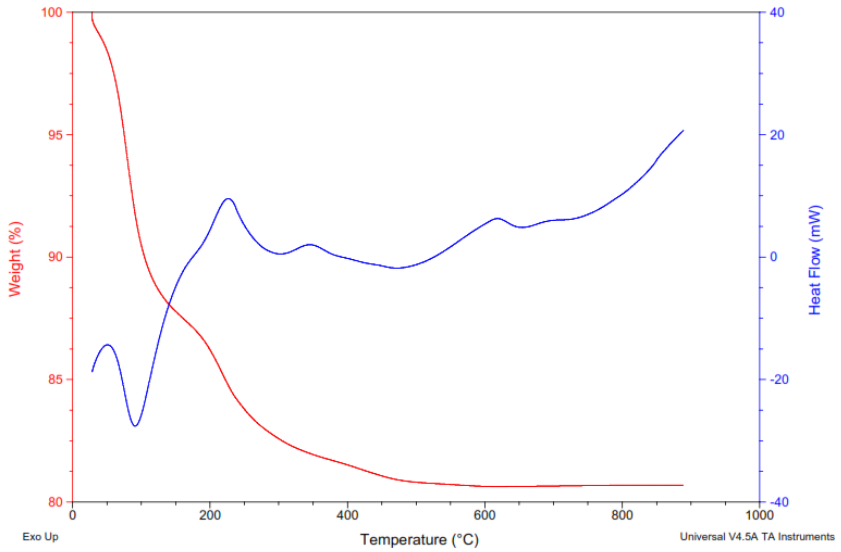

Fig. S1 TGA of Titania Sol

Thermogravimetric curve of as synthesized raw titania sample is shown in Fig. S1. Initial stage degradation below 150 °C is associated with weight loss owing to desorption of physisorbed water and ethanol present either on the wall or on the pores with weight loss of about 11%. The second degradation occurring from 200 to 500 °C is associated with the removal of organic CTAB surfactant with weigh loss of about 7 %. The removal of CTAB micelles from the titania structure leads to the formation of mesoporous (Dabler et al., 1988). Consequently, after 500 °C consistent mass of about 82 % is found to be retained.

The diffractogram results of both raw titania and calcined titania are shown in Figure. S2. The crystalline nature of calcined sample dominates as compared to the raw titania. This is due to high degree of crystallization achieved through calcination, which in turn leads to the formation of rutile and anatase phases of titania. The resulted peaks are in good agreement with the JCPDS no.: 21-1272 and 21-1276 [39, 40]. The diffraction peaks at 25.4°, 36.2°, 48.1° and 54.5°, 62.8° indicate the anatase phase which corresponds to the (101), (103), (200) and (105), (204) planes respectively. Further, the diffraction peaks at 27.7°, 41.4°, 56.7°, 69.0° indicating the rutile phase that corresponds to the (110), (111),

(220) and (301) planes respectively. The resulted peaks are in good agreement with the JCPDS no.: 21-1272 and 21-1276 [2, 3].

Fig. S3 illustrates the Raman spectra in which the peaks obtained at 147, 401, 519 and 638 cm^{-1} are assigned to the E_g, $B1_g$, $A1_g$ and E_g modes respectively, in the anatase phase. Even after calcinations, it is observed that there is no change in the vibration mode, which is due to the external vibration of well associated long-range order anatase phase appeared at 147 cm^{-1}(Chen and Mao, 2007, Naumenko et al., 2012). The diffraction peaks at 25.4°, 36.2°, 48.1° and 54.5°, 62.8° indicate the anatase phase which corresponds to the (101), (103), (200) and (105), (204) planes respectively. Further, the diffraction peaks at 27.7°, 41.4°, 56.7°, 69.0° indicating the rutile phase that corresponds to the (110), (111), (220) and (301) planes respectively. The resulted peaks are in good agreement with the JCPDS no.: 21-1272 and 21-1276 [2, 5].

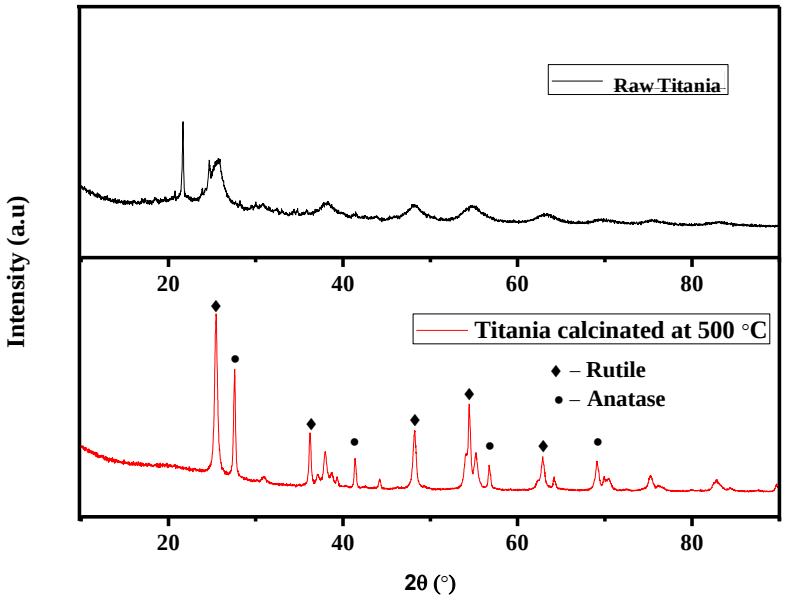

Fig. S2 XRD of raw titania and calcined samples

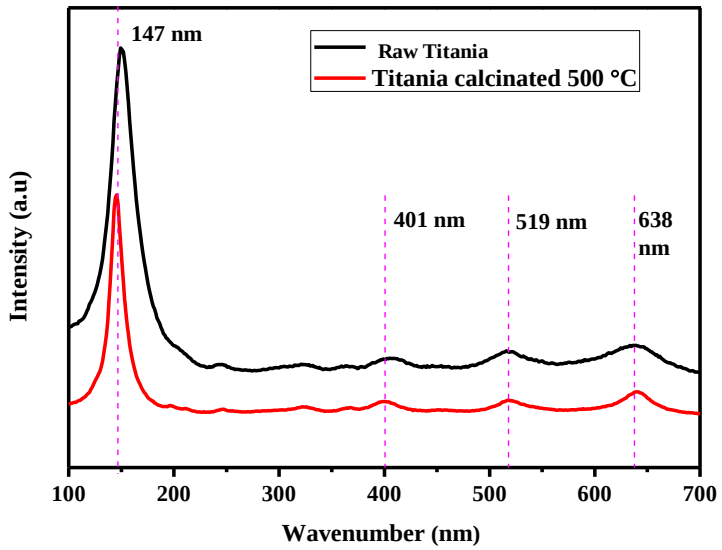

Fig. S3 Raman spectra of raw titania and calcined samples

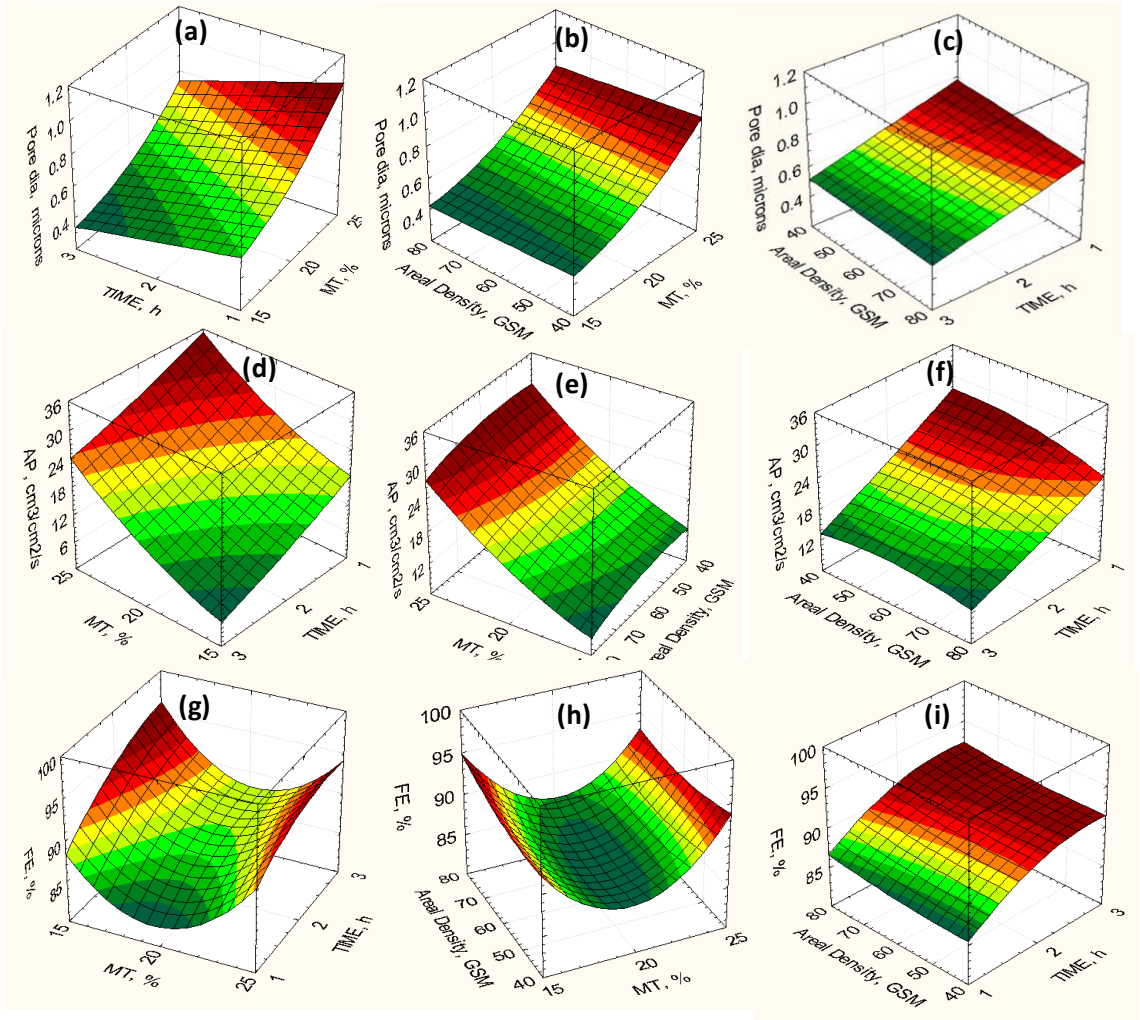

Fig. S4a Pore size variation with respect to a) MT % (b) Areal density, c) spinning time, d) Air permeability variation with respect to MT %, e) Areal density, f) Spinning time, g) Filtration efficiency variation with MT %, h) Areal density, i) Spinning time

The variation of pore size with respect to MT %, spinning time and GSM is shown in Fig. S4(a-b). Fig. S4a illustrates the variation of pore size against MT ratio. The pore size increases with increase in MT ratio, which is likely due to increase in fiber diameter w.r.t MT percentage. Further, pore size variation with respect to areal density shows no significant variation (Fig. S4b). However, the increase in spinning time decreases the pore size (Fig. S4c), which is due to continuous spinning thereby deposited more layers of

composite fibre, which in turn ultimately reduces the mean pore size of the resulted composites.

Subsequently, the inflsuence of MT %, spinning time and GSM for air permeability (AP) of composite is shown in Fig. S4(d-f). It is shown that the increase in MT % has no significant change in the air permeability and hence the mesoporous of titania favorably provides more intra-porous network in the resulted composite fibrous and in turn allows the air medium irrespective of its concentration. It is observed that low timing favors higher air permeability. However, increase in the spinning time decreases the permeability value, which is due to excess deposition of fibrous leading to retardation of the air to pass through. Further, the increase in areal density also resulted lesser air permeability.

The effect of variation of filtration efficiency with respect to MT %, areal density and spinning time was carried out and the graphs are shown in Fig. S4(g-i). The 15 % of MT embedded nanofibrous composite membrane shows higher filtration efficiency as compared to 20 % MT. This is due to increase in fibrous diameter and formation of extra pores in the fibrous composite membrane with 20 % MT. Further increase in concentration of MT from 20 to 25 wt %, the FE increases. This is due to surface charges of MT play a crucial role in preventing the aerosol during air filtration. Surface charges of the resulted MT/PAN are tuned to be suitable for the adsorption of NaCl aerosol particles, which can form stern electric double layer structures. Thus, the result clearly demonstrates the role of concentration of MT and surface charge density towards the particulate matter filtration. The effect of spinning time significantly influences the FE. Increase in spinning time increases the FE irrespective of its MT %. Comparing the 15 and 25 % MT with 1 h electro-spinning shows increase FE than that of 20 % MT. This is due to that the 20 % MT incorporated fibrous possess larger pore size and insufficient MT concentration. 15 % MT loaded fibres shows higher FE than 20 % MT loaded fibres with 1 h electrospinning. This phenomenon is due to smaller fibrous dimension (diameter) and pore size of the resulted sample. It is ascertained that the effect of areal density has minimal influence in FE.

References

1. Daßler A, Feltz A, Jung J, et al (1988) Characterization of rutile and anatase powders by thermal analysis. J Therm Anal 33:803–809. https://doi.org/10.1007/BF02138591

2. Pusit Pookmanee, Sukon Phanichphant (2009) Titanium dioxide powder prepared by a sol-gel method. J Ceram Process Res 10:167–170. https://doi.org/10.1108/JFRC-02-2017-0019

3. Zhou J, Zhao G, Song B, Han G (2011) Solvent-controlled synthesis of three-dimensional TiO2 nanostructures via a one-step solvothermal route. CrystEngComm 13:2294–2302. https://doi.org/10.1039/c0ce00793e

4. Naumenko A, Gnatiuk I, Smirnova N, Eremenko A (2012) Characterization of sol-gel derived TiO2/ZrO2films and powders by Raman spectroscopy. In: Thin Solid Films. pp 4541–4546

5. Wang K, Wei M, Morris MA, et al (2007) Mesoporous titania nanotubes: Their preparation and application as electrode materials for rechargeable lithium batteries. Adv Mater 19:3016–3020. https://doi.org/10.1002/adma.200602189